HHS Public Access

Author manuscript

*Nat Chem*. Author manuscript; available in PMC 2017 June 19.

Published in final edited form as:

*Nat Chem*. 2017 April ; 9(4): 333–340. doi:10.1038/nchem.2686.

# Atomically precise organomimetic cluster nanomolecules assembled *via* perfluoroaryl-thiol $S_NAr$ chemistry

**Elaine A. Qian**[1,2,4], **Alex I. Wixtrom**[1], **Jonathan C. Axtell**[1], **Azin Saebi**[1], **Dahee Jung**[1,4], **Pavel Rehak**[3], **Yanxiao Han**[3], **Elamar Hakim Moully**[1], **Daniel Mosallaei**[1], **Sylvia Chow**[1], **Marco S. Messina**[1,4], **Jing Yang Wang**[1], **A. Timothy Royappa**[5], **Arnold L. Rheingold**[6], **Heather D. Maynard**[1,4], **Petr Král**[3,7,8], and **Alexander M. Spokoyny**[1,4,*]

[1]Department of Chemistry and Biochemistry, University of California, Los Angeles, 607 Charles E. Young Drive East, Los Angeles, California 90095, USA.

[2]Department of Bioengineering, University of California, Los Angeles, 410 Westwood Plaza, Los Angeles, California 90095, USA.

[3]Department of Chemistry, University of Illinois at Chicago, 845 West Taylor Street, Chicago, Illinois 60607, USA.

[4]California NanoSystems Institute, University of California, Los Angeles, 570 Westwood Plaza, Los Angeles, California 90095, USA.

[5]Department of Chemistry, University of West Florida, 11000 University Parkway, Pensacola, Florida 32514, USA.

[6]Department of Chemistry and Biochemistry, University of California, San Diego, 9500 Gilman Drive, La Jolla, California 92093, USA.

[7]Department of Physics, University of Illinois at Chicago, 845 West Taylor Street, Chicago, Illinois 60607, USA.

[8]Department of Biopharmaceutical Sciences, University of Illinois at Chicago, 833 South Wood Street, Chicago, Illinois 60612, USA.



*Corresponding author: Alexander M. Spokoyny, spokoyny@chem.ucla.edu, Phone: (+1) 310-357-1327.

**Author contributions**

A.M.S. conceived the concept and supervised and guided the research. E.A.Q. and A.M.S. designed the experiments; E.A.Q. performed the majority of the experimental work. A.I.W., J.Y.W., J.C.A., and A.S. contributed to the synthesis of **2** and **3**. A.T.R and A.L.R. performed the crystallographic characterization of compound **3**. A.S., E.H.M., and D.M. contributed to the synthesis of **2j** and **3j**. S.C. assisted with optimizing the reaction conditions of **2**/**3 a–f**, **i**, **l**. A.I.W. and E.H.M. contributed to the purification of the OCNs. D.J. conducted and interpreted the TEM experiments. M.S.M. and H.D.M. assisted with the GPC experiments. Y.H., P.R., and P.K. designed, conducted and interpreted the computational experiments. E.A.Q., A.I.W., and A.M.S. co-wrote the manuscript. All authors commented on the manuscript during its preparation.

**Additional information**

Supplementary information is available in the online version of this paper.

**Competing financial interests**

The authors declare no competing financial interests.

**Data availability**

The crystallographic data have been deposited at the Cambridge Crystallographic Data Centre (CCDC) as CCDC 1493022 (2 at 100 K) & 1511361 (3 at 100 K) and can be obtained free of charge from the CCDC via www.ccdc.cam.ac.uk/getstructures.

## Abstract

The majority of biomolecules are intrinsically atomically precise, an important characteristic that enables rational engineering of their recognition and binding properties. However, imparting similar precision to hybrid nanoparticles has been challenging due to inherent limitations of the existing chemical methods and availability of properly designed functional building blocks. Here we report a new approach to form atomically precise and highly tunable hybrid nanomolecules with well-defined three-dimensionality. Perfunctionalization of atomically precise clusters with pentafluoroaryl-terminated linkers produces size-tunable rigid cluster nanomolecules. These species are amenable to facile modification with a variety of thiol-containing molecules and macromolecules. Assembly proceeds at room temperature within hours under mild conditions, and the resulting nanomolecules exhibit high stabilities due to their full covalency. We further demonstrate how these nanomolecules grafted with saccharides can exhibit dramatically improved binding affinity toward a protein. Ultimately, the developed strategy allows the rapid generation of precise molecular assemblies for investigating multivalent interactions.

Natural systems feature very complex three-dimensional molecular architectures that can interact with a high degree of specificity and fidelity. Among the well-established interaction modes, multivalency has been known to enable myriad biological events by strengthening individually weak interactions between biomolecules that are either native or foreign to the organism[1]. Multivalent interactions can be found in such diverse processes as infection (viral/bacterial proteins–cell receptors), immune recognition (antibodies–cell receptors/antigens, cytokines–cell receptors), and gene expression regulation (transcription factors–DNA), due to the higher avidity and better recognition compared to the corresponding monovalent bindings[1,2].

Inspired by nature's design, chemists have taken an interest in developing synthetic multivalent ligands with the ability to bind specific target receptors with high affinity for the purposes of 1) elucidating the mechanistic details of multivalent interactions and 2) promoting or inhibiting biological interactions of interest[3]. Many examples of synthetic scaffolds have emerged over the past several decades[4–18], including but not limited to polymeric nanoparticles[4,5], dendrimers[6,7], and hybrid nanoparticles[8–16]. Specifically, the advent of nanotechnology and the development of surface-functionalized metal nanoparticles has provided an extremely powerful class of multivalent scaffolds. For example, gold nanoparticles (AuNPs) capped with thiolated ligands can feature biocompatibility and stability, enabling them for applications requiring binding and recognition capabilities[10,11]. Hybrid AuNP systems are especially attractive due to the synthetic ease of producing systems that are well-defined and tunable in size. Nevertheless, it is well known that thiolated ligands often can desorb or undergo exchange processes with other surfactants in solution over short periods of time, and furthermore, various electrochemical conditions or elevated temperatures (>60 °C) dramatically accelerate these processes[10,19–22]. These events can be explained primarily by the relatively weak nature of the gold–thiolate bond (40–50 kcal/mol)[19]. Thiol ligand-exchange processes also readily occur on smaller Au-based cluster molecules (≤5 nm), potentially limiting the ability of researchers to create atomically precise hybrid nanomolecules that remain compositionally well-defined under biologically relevant conditions (*e.g.* in serum)[21,23].

Here we report a new strategy for building robust atomically precise hybrid nanomolecules using air-stable inorganic clusters[24–28] densely decorated with perfluoroaromatic functional groups. Using this organomimetic strategy[29], we show that one can mimic the rigid surface of a Au-based nanoparticle core while producing assemblies that are fully covalent and thus stable under relatively harsh conditions (Fig. 1). Specifically, we demonstrate how dodecaborate clusters[29,31–36] featuring a dense layer of rigid pentafluoroaryl functional groups can serve as excellent scaffolds for constructing atomically precise, multivalent organomimetic cluster nanomolecules (OCNs). The perfluoroaryls are able to undergo facile "click"-like nucleophilic aromatic substitution ($S_NAr$) with a wide range of thiols at room temperature within hours, creating robust carbon–sulfur bonds (80–90 kcal/mol)[37], thereby producing nanomolecules decorated with well-defined functional surfaces. This approach affords the functional advantages of using dendrimers while at the same time mimicking the synthetic ease with which thiol-capped AuNPs are normally constructed. Unlike the majority of dendritic scaffolds[38,39], the resulting assemblies are highly rigid and can be synthesized and purified within hours. Furthermore, these OCNs are purely covalent and therefore feature improved stability in serum and various pH environments. Finally, we demonstrate the first example of using hybrid inorganic cluster scaffold as a highly competent multivalent recognition platform for binding a protein system.

## Results and discussion

Given the high reactivity of the perfluoroarenes with thiol-based nucleophiles[40–44], we hypothesized that perfluoroaryl-thiol $S_NAr$ chemistry could be utilized to conjugate various thiolated groups onto perfluoroaryl-containing clusters efficiently under mild conditions at room temperature. Our laboratory has recently reported a rapid perfunctionalization strategy of $[B_{12}(OH)_{12}]^{2-}$ cluster (**1**) originally discovered by Hawthorne[31–34] featuring a wide scope of substituents[35]. Using this method, we synthesized perfunctionalized clusters grafted with rigid linkers containing peripheral pentafluoroaryl moieties (Fig. 2a). Specifically, perfunctionalized cluster scaffolds **2** and **3** can be synthesized in good yields under 30 minutes and isolated after purification by silica gel column chromatography in their neutral form as air-stable solids soluble in the majority of common polar organic solvents (Supplementary Information, pages 9–12). The single crystal X-ray structures of **2** and **3** reveal the highly rigid nature of these scaffolds (Fig. 2b and 2c, respectively). Importantly, by virtue of using size-tunable linker precursor in the synthesis of **2** and **3**, the resulting rigid cluster species can be rationally controlled in size (**2** is approximately 1.9 and **3** is about 2.7 nm lengthwise, as measured from the single crystal structures). These clusters represent a new class of atomically precise scaffolds that offer unique rigidity and structural covalency, making them topologically reminiscent of both dendrimers and small metal nanoparticles.

To test our hypothesis that **2** and **3** could be fully functionalized by thiols *via* $S_NAr$ reaction, we commenced conjugation studies between **2** and 1-hexanethiol (**a**). Cluster **2** was mixed with 12 eq. of thiol **a** in dimethylformamide (DMF) in the presence of base and left stirring under $N_2$ atmosphere to mitigate the undesired oxidation of the thiol reagent. Notably, the initially dark red solution quickly turned colorless. $^{11}B$ NMR spectroscopy of this colorless solution revealed a singlet resonance at $\delta$ −15 characteristic of a reduced cluster in a $[\mathbf{2}]^{2-}$ oxidation state[35,36], which is consistent with the reducing capacity of the thiolate species

when exposed to $[\mathbf{2}]^0$ (Fig. 2d). Therefore, for all subsequent optimization studies we utilized an extra equivalent of the thiol reagent to account for this reduction (Supplementary Table 1). $^{19}$F NMR spectroscopy was utilized to monitor the conversion of **2** to **2a**, given the diagnostic change associated with this transformation (Fig. 2d – disappearance of the *para*-F resonance and significant downfield shift of the *meta*-F resonances in **2a** compared to the starting material **2**). A base screen identified potassium carbonate ($K_2CO_3$) as the optimal reagent leading to the substantial conversion resulting in the formation of perfunctionalized cluster **2a** (Supplementary Table 1, entry 4). After additional optimization using $K_2CO_3$, we found that using 13.3 eq. of **a** and 30 eq. of $K_2CO_3$ resulted in a nearly quantitative (>99%) substitution of **2**, producing the 12-fold substituted OCN **2a** (Table 1, entry 1, Fig. 2d). The crude product was dried and then purified *via* silica gel column chromatography and isolated as an oily substance in 70% yield (Supplementary Information, pages 13–14). Electrospray ionization-high resolution mass spectrometry (ESI-HRMS), $^1$H, $^{11}$B, and $^{19}$F NMR spectroscopy of purified **2a** are consistent with its proposed structure and composition (Supplementary Information, pages 51–55). We further found that **2** could be fully conjugated with aromatic (**b**) and benzylic (**c**) thiols. Both reactions proceeded nearly quantitatively within 24 hours at room temperature using potassium phosphate ($K_3PO_4$), leading to pure OCNs **2b** and **2c** (Table 1, entries 2 and 3), respectively, after isolation in good yields (see Supplementary Information, pages 14–16 and 56–69, for details on reaction conditions, purification, and characterization). Importantly, results with **2a–c** indicate that the developed chemistry can operate with a wide range of thiol-based species spanning a significant window of nucleophilicities (pKa of aliphatic thiols is approximately 17, aromatic – 10). Overall, these experiments suggest that using the developed method, it is possible to rapidly assemble OCNs *via* $S_NAr$ chemistry under very mild and operationally simple conditions mimicking the simplicity of the thiol-capped AuNPs assembly. Furthermore, unlike the previously developed Huisgen “click” cycloaddition and carbamate functionalization strategies of inherently non-rigid $B_{12}$-based clusters, which require elevated temperatures, long reaction times (days) and a large excess of reagents (4–5 fold per vertex), the perfluoroaryl-thiol $S_NAr$ chemistry described here proceeds using significantly milder conditions[33,34].

Thiol-capped AuNP constructs are also extremely attractive given the chemical orthogonality of the gold-thiol interaction compared to other ligands, which provides an opportunity to use a wide variety of unprotected thiol reagents for facile and programmable self-assembly. Therefore, we decided to probe the degree to which $S_NAr$ chemistry on perfluorinated clusters can mimic this attractive feature. To evaluate the thiol-selectivity of our approach, we performed conjugation reactions between **2** and thiols featuring additional nucleophilic groups such as alcohols and amines. Consistent with the previous work by Pentelute and co-workers with unprotected peptides[43,44], we found that the model thiol species (**d–f**) all reacted with **2** through the thiol site selectively to form the desired perfunctionalized OCNs **2d–f** (Table 1, entries 4–6) within 24 hours as confirmed by $^{19}$F NMR spectroscopy (see Supplementary Information, pages 16–19 and 139–159, for details on reaction conditions, purification, and characterization). This finding is important as it suggests that this chemistry can be used to selectively conjugate thiol reagents containing multiple nucleophilic functional groups and fundamentally takes advantage of the mild

conditions developed here, which allow one to guide the kinetic selectivity between the thiol and pentafluoroaryl fragment[42–44]. Most importantly, this chemoselectivity is reminiscent of that observed in the assembly of thiol-capped AuNPs.

With the successful perfunctionalization of **2** (*vide supra*), we hypothesized that the larger-sized cluster **3** could not only be perfunctionalized with the same thiols to create a new generation of OCNs that are modularly extended in size, but could also accommodate 12-fold conjugation with bulkier substrates. Indeed, under the same conditions as described above for functionalization of **2**, cluster **3** undergoes clean and facile perfunctionalization chemistry with thiols **a–f**, yielding **3a–f** (Table 1, entries 7–12 and Supplementary Information, pages 25–31 and 118–159). Importantly, when using **3** instead of **2**, we observed a significantly faster conversion rate leading to perfunctionalized clusters (under six hours versus 24 hours), consistent with the surface of **3** being less sterically encumbered than **2**. Therefore, using **3** allowed full substitution with a bulky cysteine derivative (**g**) as well as a small, unprotected peptide sequence C-A-G (**h**), yielding **3g** and **3h**, respectively (Table 1, entries 13 and 14; Supplementary Information, pages 31–33, 160–173, and 222).

Next, to test whether more complex molecular architectures could also be introduced onto the clusters, we turned our attention to poly(ethylene glycol) (PEG)[4,22,45,46]. Complete 12-fold conjugation between **2** and commercially available mPEG-thiol ($MW_{avg}$ = 356 Da) occurred within 24 hours at room temperature, yielding OCN **2i** (Table 2, entry 1; Supplementary Information, pages 19–20 and 91–97). Subsequently, larger mPEG-thiols ($MW_{avg}$ = 766 Da and 2,000 Da) were tested and similarly afforded **2j** and **2k**, respectively, in quantitative conversions based on $^{19}F$ NMR spectroscopy (Table 2, entries 2 and 3; Supplementary Information, pages 20–23 and 98–110). As expected, PEGylation conferred considerable hydrophilicity to these clusters: **2i–k** are readily soluble in water. Due to the full covalency of PEGylated OCNs, we hypothesized that these species should be structurally stable under biological conditions. Using **2i** as a model, we conducted stability studies in biologically relevant media (Supplementary Information, pages 204–221). A purified sample of **2i** was exposed to cell culture media containing fetal bovine serum (FBS) for five days at room temperature, and no changes or degradation products were observed by monitoring this sample *via* $^{19}F$ and $^{11}B$ NMR spectroscopy. Similarly, no degradation occurred when this sample was incubated for an additional five days at 37 °C. Importantly, samples of **2i** were dissolved in buffers of various pH (5, 7, and 9) for five days, and these were found to remain structurally intact as well. These results suggest that OCNs retain their structural integrity under the wide range of biologically relevant conditions. We then decided to investigate the stability of the conjugation linkage between the cluster core and the thiol. Given the full covalency of **2i**, we expected that it should not undergo ligand-exchange, a process that commonly occurs with many ligand-capped AuNPs[22]. Significantly, no thiol-exchange occurred when **2i** (0.8 mM) was exposed to 2-mercaptoethanol (20 mM) over a period of 11 days. Similar results were obtained with 2 mM glutathione (GSH). Overall, these experiments clearly demonstrate that the OCNs constructed *via* the $S_NAr$ approach feature superior robustness compared to many AuNP-based assemblies[10,21].

PEGylated OCNs were characterized by a number of techniques to ensure their proposed nearly monodisperse composition (while the OCN cores are monodisperse, the PEG chains

used in this study feature some compositional variability due to the inherent limitations of PEG oligomer synthesis)[47]. First, we conducted 2D diffusion-ordered (DOSY) $^1$H NMR spectroscopy experiments with purified samples of **2i–k** and the more extended OCNs **3i–k** (Table 2, entries 5–7 and Supplementary Information, pages 33–36 and 174–190) in $D_2O$ (see 2D DOSY method and plots in the Supplementary Information, pages 6 and 198–203). Based on the diffusion constants obtained from these DOSY experiments, the respective hydrodynamic diameters were estimated (Fig. 3a). As expected, the results reveal a gradual increase in the sizes of the PEGylated clusters, both as a function of the cluster core size (from **2** to **3**) and the length of the PEG chain used. We noted that the size of **3i** measured by 2D DOSY $^1$H NMR spectroscopy was larger than expected, most likely due to aggregation under the conditions the measurement was performed – suggesting the small number of PEG units in **3i** could not fully stabilize the hydrophobic core against self-aggregation. To determine the size of a single non-aggregated OCN **3i**, we performed additional transmission electron microscopy (TEM) experiments on **3i** (Fig. 3b and Supplementary Information, page 6). The TEM images reveal the presence of nearly monodisperse particles with an average size of 1.9 nm, which is in agreement with the expected value for a non-aggregated single particle. Consistent with these results, gel permeation chromatography (GPC) traces of **2k** and **3k** in water (Fig. 3c) also reveal nearly monodisperse samples ($Đ$ = 1.003 ± 0.02, 1.081 ± 0.007, respectively; Supplementary Information, page 6). Furthermore, we performed molecular dynamics (MD) simulations of species **2i–k** and **3i–k** in water and calculated their hydrodynamic radii and radii of gyration (snapshots after 21 ns in Fig. 3d; Supplementary Information, pages 223–231 and movies). The results are in good agreement with the non-aggregated OCN sizes measured by TEM, and furthermore exhibit a trend similar to the one observed by 2D DOSY $^1$H NMR spectroscopy. A small discrepancy arises between the sizes estimated based on computational studies/TEM and 2D DOSY $^1$H NMR spectroscopy and is likely due to some aggregation of the particles under the conditions employed in 2D DOSY $^1$H NMR spectroscopy experiments. Overall, our measurements clearly show that using the developed $S_NAr$ assembly strategy, one can rationally prepare robust and nearly monodisperse samples of size-tunable PEGylated OCNs.

After demonstrating the scope of the developed chemistry with various classes of thiols, we next aimed to coat the scaffold clusters with recognition moieties in order to develop OCNs capable of multivalent binding interactions. In nature, multivalent glycoconjugates such as glycoproteins and glycolipids can bind lectins with relatively high avidity, thereby bypassing the fundamental limitation of weak monosaccharide binding (dissociation constants ($K_D$) ranging between mM and μM)[38,48–52]. We hypothesized that cluster **2** and **3** can serve as a rigid, tunable scaffold for three-dimensional, precise display of carbohydrates. Using commercially available carbohydrate precursor 1-thio-β-D-glucose tetraacetate, we have synthesized functionalized OCNs **2l** and **3l** featuring 12 appended glucose molecules (Table 2, entries 4 and 8; Fig. 4a; Supplementary Information, pages 24–25, 36–37, 111–117, and 191–197). We then conducted surface plasmon resonance (SPR) experiments with a Biacore T100 instrument to monitor and quantify binding interactions between the glycosylated OCN **2l** and a model lectin Concanavalin A (ConA) at pH 7.4 (Supplementary Information, pages 6–7). ConA was covalently attached to the Au-coated sensor chip's dextran layer *via* conventional amide coupling[53], and binding between ConA and the injected analyte was

measured as a change in refractive index (RI) and expressed in response units (RU). From the binding sensorgrams (Fig. 4b), it is clear that the measured binding response was dependent on the concentration of **2l** in the injected sample. Furthermore, when two controls (**2i** and D-glucose) were injected at the highest mass concentration of **2l** shown (2.0 mg/L), minimal to no binding was observed. When the binding curves of **2l** were fitted to the Langmuir 1:1 binding model, the $K_D$ value was estimated to be 54 nM, which corresponds to a 6,500-fold increase in affinity when compared to the $K_D$ between ConA and methyl D-glucopyranoside[53]. These results are consistent with the $K_D$ value previously reported by Munoz and co-workers between ConA and a 3rd generation D-glucose-functionalized glycodendrimer (15.8 nM, 27 saccharides). This result is significant since it demonstrates that a similar multivalent effect can be achieved by using a rigid OCN scaffold featuring significantly fewer (12 vs. 27) saccharides. Furthermore, compared to the glycodendrimer used in the work of Munoz and co-workers, which requires 8 synthetic steps, glycosylated OCNs can be rapidly constructed in 3 steps with an $S_NAr$ conjugation done under 24 hours (Huisgen click cycloaddition conjugations on large dendritic assemblies normally take several days for completion)[54]. Lastly, we note that the OCNs generated here are fully covalent and therefore feature enhanced stability properties compared to the species synthesized *via* coordination-based self-assembly[55].

We hypothesized that the glycosylated OCN's dramatically enhanced affinity over D-glucose toward ConA can be explained by the cluster glycoside effect[38], and in order to better understand the mechanistic details of binding between **2l** and ConA, we performed MD simulations of the interactions between **2l** and ConA in water (see snapshots of the simulations in Fig. 4c–f; Supplementary Information, pages 231–237 and movies). Our calculation results are consistent with the experimental observations – that **2l** exhibits much higher affinity than the monovalent D-glucose molecule toward ConA's saccharide-binding sites. Furthermore, the higher affinity can be attributed to the multivalent statistical/rebinding effect provided by the densely functionalized surface filled with monosaccharide ligands positioned around the OCN cluster[3,53].

## Conclusions

We have developed a new strategy that allows rapid assembly of fully covalent nanoparticles with atomic precision. Specifically, we demonstrated that the rigid clusters densely decorated with perfluoroaryl-containing functional groups undergo efficient conjugation with various thiols *via* $S_NAr$ chemistry under very mild conditions at room temperature. Importantly, this chemistry is operationally reminiscent of the chemoselective assembly conditions associated with thiol-capped gold nanoparticles (AuNPs). Furthermore, similarly to thiol-capped AuNPs, these organomimetic cluster nanomolecules (OCNs) can be easily tuned in size and surface chemistry by choosing a specific thiol reagent. OCNs exhibit dramatically improved structural stability under a wide range of biologically relevant conditions due to the full covalency of all bonding interactions comprising these nanomolecules. Finally, using this assembly strategy we show how one can design and synthesize nanomolecules featuring a three-dimensional densely packed layer of saccharides that can participate in multivalent binding with a natural lectin leading to a dramatic increase in binding affinity. This work ultimately opens a new avenue for creating highly tailored

synthetic mimics of ligand-capped AuNPs featuring rigid and fully covalent atomically precise assemblies.

## Supplementary Material

Refer to Web version on PubMed Central for supplementary material.

## Acknowledgments

A.M.S. acknowledges the UCLA Department of Chemistry and Biochemistry for start-up funds, 3M for a Non-Tenured Faculty Award and the American Chemical Society Petroleum Research Fund (56562-DNI3) for the Doctoral New Investigator Grant. E.A.Q. thanks the USPHS of the NIH for the Predoctoral Training Fellowship through the UCLA Chemistry-Biology Interface Training Program under the National Research Service Award (T32GM008496). A.S. is funded by the CARE Scholars Programs (NIH grant GM055052). M.S.M. is grateful to the NSF for the Bridge-to-Doctorate and the Predoctoral (GRFP) fellowships. P.K. acknowledges the NSF Division of Materials Research grants 1309765 and 1506886. H.D.M. thanks the NSF (CHE-1507735) for funding. We thank UCLA Molecular Instrumentation Center for mass spectrometry and NMR spectroscopy (NIH grant 1S10OD016387-01, NSF grant CHE-1048804). We also thank the Electron Imaging Center for Nanomachines at the UCLA CNSI for electron microscopy (NIH grant 1S10RR23057 to ZHZ) and the UCLA Biochemistry Instrumentation Facility for SPR measurements.

## References

1. Mammen M, Choi S-K, Whitesides GM. Polyvalent interactions in biological systems: implications for design and use of multivalent ligands and inhibitors. Angew. Chem., Int. Ed. 1998; 37:2754–2794.
2. Kiessling LL, Gestwicki JE, Strong LE. Synthetic multivalent ligands as probes of signal transduction. Angew. Chem., Int. Ed. 2006; 45:2348–2368.
3. Jones LH. Recent advances in the molecular design of synthetic vaccines. Nature Chem. 2015; 7:952–960. [PubMed: 26587710]
4. Elsabahy M, Wooley KL. Design of polymeric nanoparticles for biomedical delivery applications. Chem. Soc. Rev. 2012; 41:2545–2561. [PubMed: 22334259]
5. Rao JP, Geckeler KE. Polymer nanoparticles: preparation techniques and size-control parameters. Prog. Polym. Sci. 2011; 36:887–913.
6. Tomalia DA, et al. A new class of polymers: starburst-dendritic macromolecules. Polym. J. 1985; 17:117–132.
7. Hawker CJ, Frechet JMJ. Preparation of polymers with controlled molecular architecture. A new convergent approach to dendritic macromolecules. J. Am. Chem. Soc. 1990; 112:7638–7647.
8. Farokhzad OC, Langer R. Impact of nanotechnology on drug delivery. ACS Nano. 2009; 3:16–20. [PubMed: 19206243]
9. Peer D, et al. Nanocarriers as an emerging platform for cancer therapy. Nature Nanotech. 2007; 2:751–760.
10. Daniel M, Astruc D. Gold nanoparticles: assembly, supramolecular chemistry, quantum-size-related properties, and applications toward biology, catalysis, and nanotechnology. Chem. Rev. 2004; 104:293–346. [PubMed: 14719978]
11. Dreaden EC, Alkilany AM, Huang X, Murphy CJ, El-Sayed MA. The golden age: gold nanoparticles for biomedicine. Chem. Soc. Rev. 2012; 41:2740–2779. [PubMed: 22109657]
12. Brust M, Walker M, Bethell D, Schiffrin DJ, Whyman R. Synthesis of thiol-derivatised gold nanoparticles in a two-phase liquid–liquid system. J. Chem. Soc., Chem. Commun. 1994; 17:801–802.
13. Giljohann DA, et al. Oligonucleotide loading determines cellular uptake of DNA-modified gold nanoparticles. Nano Lett. 2007; 7:3818–3821. [PubMed: 17997588]
14. Zhao H, et al. Reversible trapping and reaction acceleration within dynamically self-assembling nanoflasks. Nature Nanotech. 2015; 11:82–88.

15. Jones MR, Seeman NC, Mirkin CA. Programmable materials and the nature of the DNA bond. Science. 2015; 347:1260901-1–1260901-11. [PubMed: 25700524]
16. Suzuki K, Sato S, Fujita M. Template synthesis of precisely monodisperse silica nanoparticles within self-assembled organometallic spheres. Nature Chem. 2010; 2:25–29. [PubMed: 21124376]
17. Heindl C, Peresypkina EV, Virovets AV, Kremer W, Scheer M. Giant rugby ball [{$Cp^{Bn}Fe(\eta^5$-$P_5)$}$_{24}Cu_{96}Br_{96}$] derived from pentaphosphaferrocene and $CuBr_6$ . J. Am. Chem. Soc. 2015; 137:10938–10941. [PubMed: 26280785]
18. Ambrogio MW, Thomas CR, Zhao Y-L, Zink JI, Stoddart JF. Mechanized silica nanoparticles: a new frontier in theranostic nanomedicine. Acc. Chem. Res. 2011; 44:903–913. [PubMed: 21675720]
19. Love JC, Estroff LA, Kriebel JK, Nuzzo RG, Whitesides GM. Self-assembled monolayers of thiolates on metals as a form of nanotechnology. Chem. Rev. 2005; 105:1103–1170. [PubMed: 15826011]
20. Hostetler MJ, Green SJ, Stokes JJ, Murray RW. Monolayers in three dimensions: synthesis and electrochemistry of ω-functionalized alkanethiolate-stabilized gold cluster compounds. J. Am. Chem. Soc. 1996; 118:4212–4213.
21. Hostetler MJ, Templeton AC, Murray RW. Dynamics of place-exchange reactions on monolayer-protected gold cluster molecules. Langmuir. 1999; 15:3782–3789.
22. MacLeod MJ, Johnson JA. PEGylated N-heterocyclic carbene anchors designed to stabilize gold nanoparticles in biologically relevant media. J. Am. Chem. Soc. 2015; 137:7974–7977. [PubMed: 26081724]
23. Häkkinen H. The gold–sulfur interface at the nanoscale. Nature Chem. 2012; 4:443–455. [PubMed: 22614378]
24. Yvon C, et al. Polyoxometalate clusters integrated into peptide chains and as inorganic amino acids: solution- and solid-phase approaches. Angew. Chem., Int. Ed. 2014; 53:3336–3341.
25. Lachkar D, Vilona D, Dumont E, Lelli M, Lacôte E. Grafting of secondary diolamides onto $[P_2W_{15}V_3O_{62}]^{9-}$ generates hybrid heteropoly acids. Angew. Chem., Int. Ed. 2016; 55:5961–5965.
26. Gouzerh P, Proust A. Main-group element, organic, and organometallic derivatives of polyoxometalates. Chem. Rev. 1998; 98:77–112. [PubMed: 11851500]
27. Müller A, Gouzerh P. From linking of metal-oxide building blocks in a dynamic library to giant clusters with unique properties and towards adaptive chemistry. Chem. Soc. Rev. 2012; 41:7431–7463. [PubMed: 22948798]
28. Li G, Wang L, Ni H, Pittman CU. Polyhedral oligomeric silsesquioxane (POSS) polymers, copolymers, and resin nanocomposites. J. Inorg. Organomet. Polym. 2002; 11:123–154.
29. Spokoyny AM. New ligand platforms featuring boron-rich clusters as organomimetic substitutents. Pure & App. Chem. 2013; 85:903–919.
30. Lee IS, Long JR, Prusiner SB, Safar JG. Selective Precipitation of prions by polyoxometalate complexes. J. Am. Chem. Soc. 2005; 127:13802–13803. [PubMed: 16201796]
31. Pitochelli AR, Hawthorne FM. The isolation of the icosahedral $B_{12}H_{12}^{-2}$ ion. J. Am. Chem. Soc. 1960; 82:3228–3229.
32. Farha OK, et al. Synthesis of stable dodecaalkoxy derivatives of *hypercloso*-$B_{12}H_{12}$ . J. Am. Chem. Soc. 2005; 127:18243–18251. [PubMed: 16366578]
33. Jalisatgi SS, et al. A convenient route to diversely substituted icosahedral closomer nanoscaffolds. J. Am. Chem. Soc. 2011; 133:12382–12385. [PubMed: 21766843]
34. Sarma SJ, Khan AA, Goswami LN, Jalisatgi SS, Hawthorne MF. A trimodal closomer drug-delivery system tailored with tracing and targeting capabilities. Chem. Eur. J. 2016; 22:12715–12723. [PubMed: 27416332]
35. Wixtrom AI, et al. Rapid synthesis of redox-active dodecaborane $B_{12}(OR)_{12}$ clusters under ambient conditions. Inorg. Chem. Front. 2016; 3:711–717. [PubMed: 27885335]
36. Messina MS, et al. Visible-light-induced olefin activation using 3D aromatic boron-rich cluster photooxidants. J. Am. Chem. Soc. 2016; 138:6952–6955. [PubMed: 27186856]
37. Haynes, WM. CRC Handbook of Chemistry and Physics. Taylor and Francis: CRC Press; 2016.

38. Lundquist JJ, Toone EJ. The cluster glycoside effect. Chem. Rev. 2002; 102:555–578. [PubMed: 11841254]
39. Moore JS, Xu Z. Synthesis of rigid dendritic macromolecules: enlarging the repeat unit size as a function of generation, permitting growth to continue. Macromolecules. 1991; 24:5893–5894.
40. Birchall JM, Green M, Haszeldine RN, Pitts AD. The mechanism of the nucleophilic substitution reactions of polyfluoroarenes. Chem. Commun. 1967; 7:338–339.
41. Becer CR, Hoogenboom R, Schubert US. Click chemistry beyond metal-catalyzed cycloaddition. Angew. Chem., Int. Ed. 2009; 48:4900–4908.
42. Becer CR, et al. Clicking pentafluorostyrene copolymers: synthesis, nanoprecipitation, and glycosylation. Macromolecules. 2009; 42:2387–2394.
43. Spokoyny AM, et al. A perfluoroaryl-cysteine $S_NAr$ chemistry approach to unprotected peptide stapling. J. Am. Chem. Soc. 2013; 135:5946–5949. [PubMed: 23560559]
44. Zhang C, et al. π-clamp-mediated cysteine conjugation. Nature Chem. 2015; 8:120–128. [PubMed: 26791894]
45. Hoffman AS. The origins and evolution of ‘controlled’ drug delivery systems. J. Control. Release. 2008; 132:153–163. [PubMed: 18817820]
46. Alconcel SNS, Baas AS, Maynard HD. FDA-approved poly(ethylene glycol)–protein conjugate drugs. Polym. Chem. 2011; 2:1442–1448.
47. Veronese FM, Pasut G. PEGylation, successful approach to drug delivery. Drug Discov. Today. 2005; 10:1451–1458. [PubMed: 16243265]
48. Dam TK, Roy R, Das SK, Oscarson S, Brewer CF. Binding of multivalent carbohydrates to Concanavalin A and *Dioclea grandiflora* lectin. Thermodynamic analysis of the “multivalency effect”. J. Biol. Chem. 2000; 275:14223–14230. [PubMed: 10799500]
49. Müller C, Despras G, Lindhorst TK. Organizing multivalency in carbohydrate recognition. Chem. Soc. Rev. 2016; 45:3275–3302. [PubMed: 27146554]
50. Muñoz A, et al. Synthesis of giant globular multivalent glycofullerenes as potent inhibitors in a model of Ebola virus infection. Nature Chem. 2016; 8:50–57. [PubMed: 27055288]
51. Bhatia S, Camacho LC, Haag R. Pathogen inhibition by multivalent ligand architectures. J. Am. Chem. Soc. 2016; 138:8654–8666. [PubMed: 27341003]
52. Bernardi A, et al. Multivalent glycoconjugates as anti-pathogenic agents. Chem. Soc. Rev. 2013; 42:4709–4727. [PubMed: 23254759]
53. Munoz EM, Correa J, Riguera R, Fernandez-Megia E. Real-time evaluation of binding mechanisms in multivalent interactions: a surface plasmon resonance kinetic approach. J. Am. Chem. Soc. 2013; 135:5966–5969. [PubMed: 23565759]
54. Fernandez-Megia E, Correa J, Rodríguez-Meizoso I, Riguera R. A click approach to unprotected glycodendrimers. Macromolecules. 2006; 39:2113–2120.
55. Kamiya N, Tominaga M, Fujita M. Saccharide-coated $M_{12}L_{24}$ molecular spheres that form aggregates by multi-interaction with proteins. J. Am. Chem. Soc. 2007; 129:3816–3817. [PubMed: 17343384]

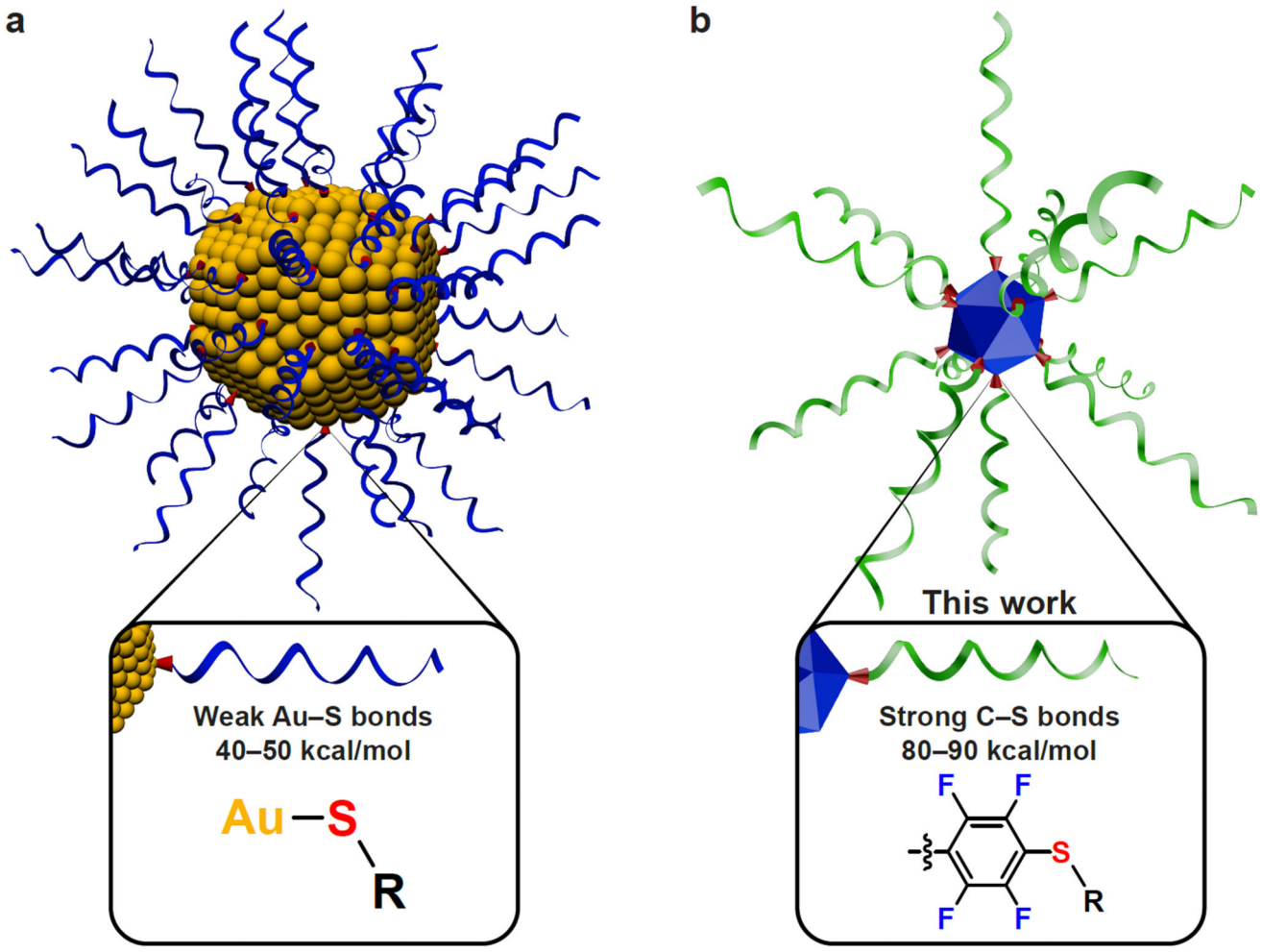


**Figure 1. Comparison of features between the thiol-capped gold nanoparticles (AuNPs) and the organomimetic cluster nanomolecules (OCNs)**

**a**, Thiol-capped AuNPs between 5 and 100 nm can be easily prepared *via* self-assembly, giving rise to polydisperse hybrid particles comprising weak, non-covalent gold–thiolate bonds (40–50 kcal/mol). These AuNPs often undergo ligand-exchange processes that can compromise the structural integrity of the particles. **b**, Uniform and robust OCNs can be efficiently assembled with atomic precision and full covalency in the size range of 2 to 10 nm *via* perfluoroaryl-thiol $S_NAr$ chemistry under mild conditions. The formed carbon–sulfur bond (80–90 kcal/mol) is significantly stronger compared to the gold-sulfur interaction, resulting in nanomolecules that feature high structural stabilities.

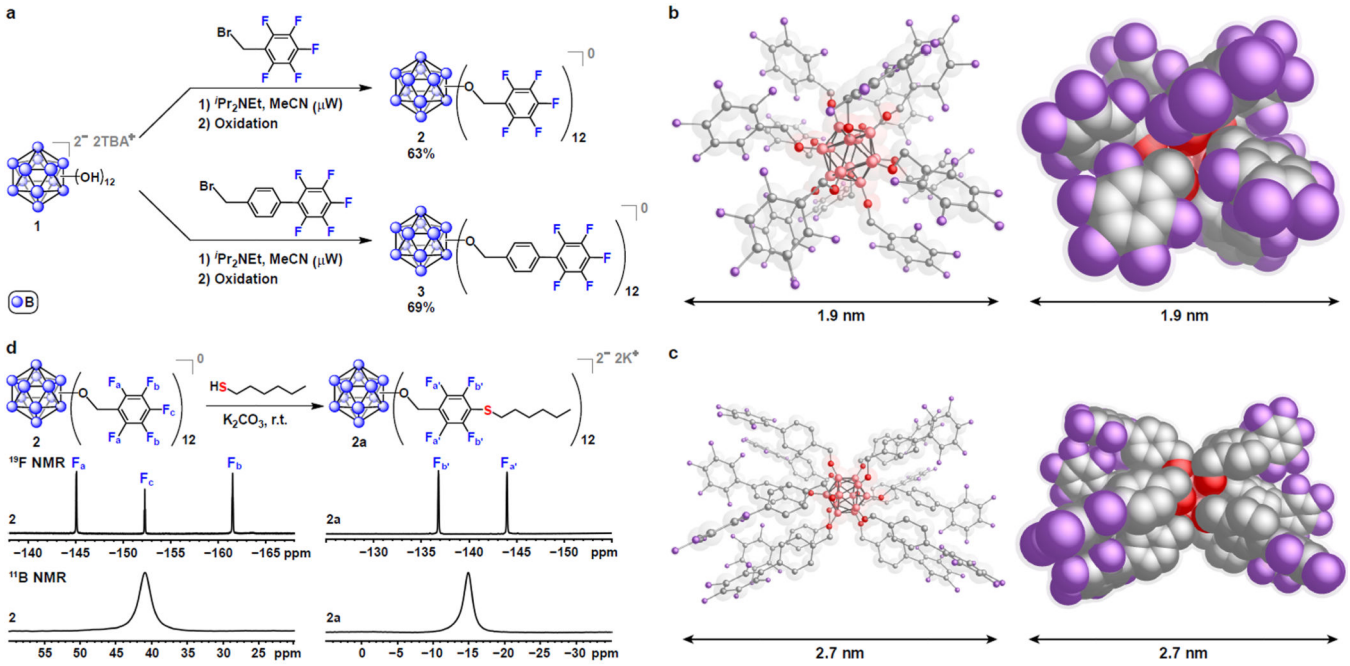


**Figure 2. Synthesis and characterization of the perfluoroaryl-perfunctionalized dodecaborate clusters and the subsequent modification with thiols**

**a**, Perfunctionalization of **1** with rigid pentafluoroaryl-terminated linkers yields pure clusters **2** and **3**, after isolation. **b**,**c**, Ball-and-stick and space-filling representations of the single crystal X-ray structures of **2** and **3**, respectively. Size measurements of the crystal structures reveal that **2** is 1.9 nm and **3** is 2.7 nm (lengthwise). Salmon = B, red = O, grey = C, purple = F. **d**, "Click"-like modification of cluster **2** with the 1-hexanethiol reagent and the corresponding $^{19}$F and $^{11}$B NMR spectra associated with the transformation from the starting material **2** to the functionalized product **2a**. Specifically, perfunctionalization of **2** with 1-hexanethiol results in a shift of the *meta*-F resonance and the complete disappearance of the *para*-F resonance as well as a characteristic upfield shift of the boron singlet resulting from the reduction of the cluster.

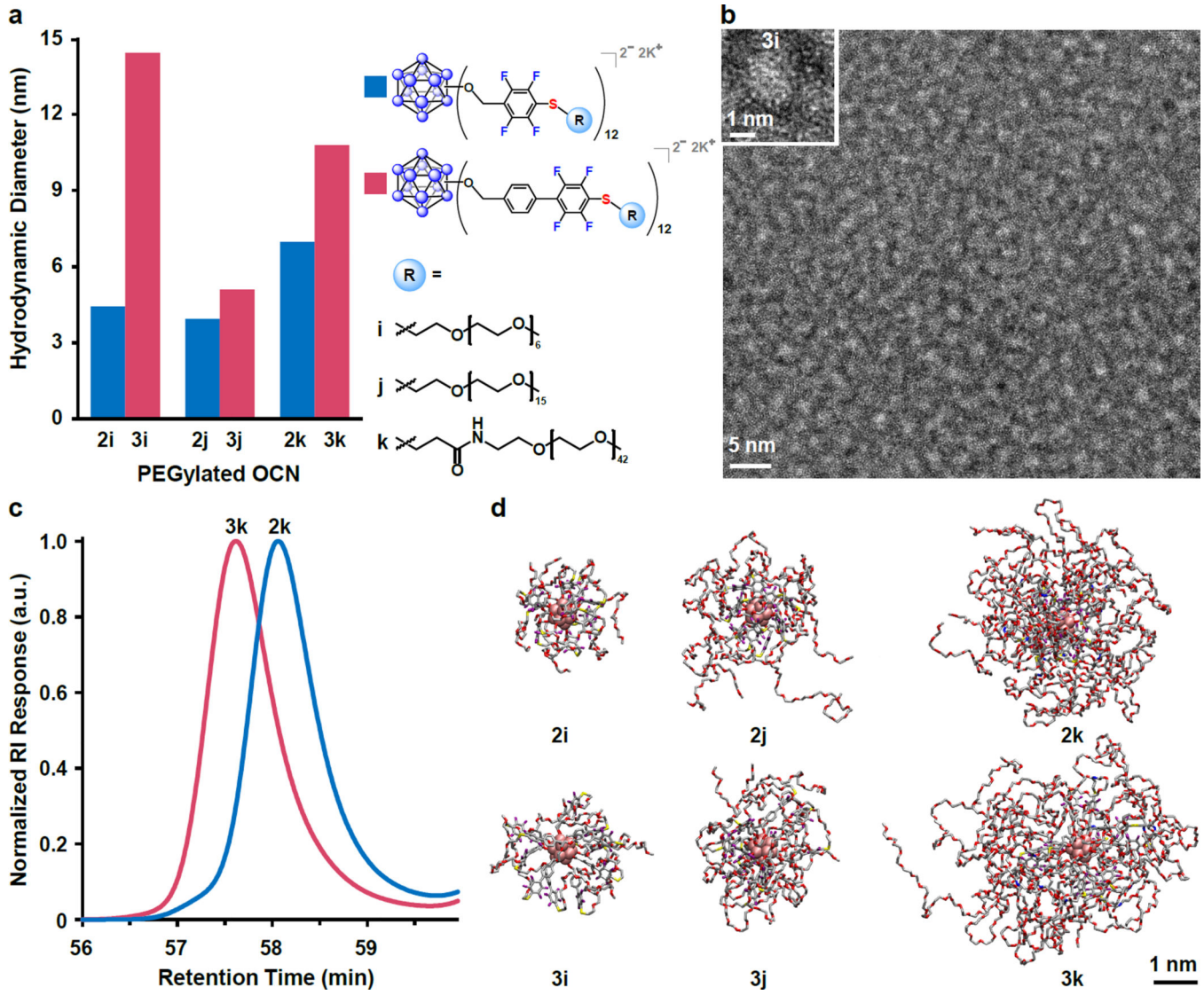


**Figure 3. Characterization of the PEGylated OCNs 2i–k and 3i–k**

**a**, Plot of the particle sizes of the PEGylated OCNs **2i–k** and **3i–k** obtained *via* 2D diffusion-ordered (DOSY) $^{1}$H NMR spectroscopy experiments. The plot reveals a trend of a gradual increase in the sizes of the OCNs both as a function of the cluster precursor dimension and the chain-length of a PEG reagent. We note that the size of **3i** is larger than expected, likely due to aggregation. **b**, Transmission electron microscopy (TEM) images of a negatively stained sample of **3i** reveal the presence of nearly monodisperse particles with an average size of 1.9 nm, consistent with the expected size of **3i**. **c**, Gel permeation chromatography (GPC) traces of **2k** and **3k** measured in water further confirm the monodispersity of the samples ($Đ$ = 1.003 ± 0.02 and 1.081 ± 0.007, respectively). RI = refractive index. **d**, Molecular dynamics (MD) calculated structures of the PEGylated nanomolecules in pure water after 21 ns (see the Supplementary Information for the movies showcasing dynamics in **2i–k** and **3i–k**) of simulation indicate a trend in the sizes of the OCNs consistent with the one observed through the 2D DOSY $^{1}$H NMR spectroscopy experiments.

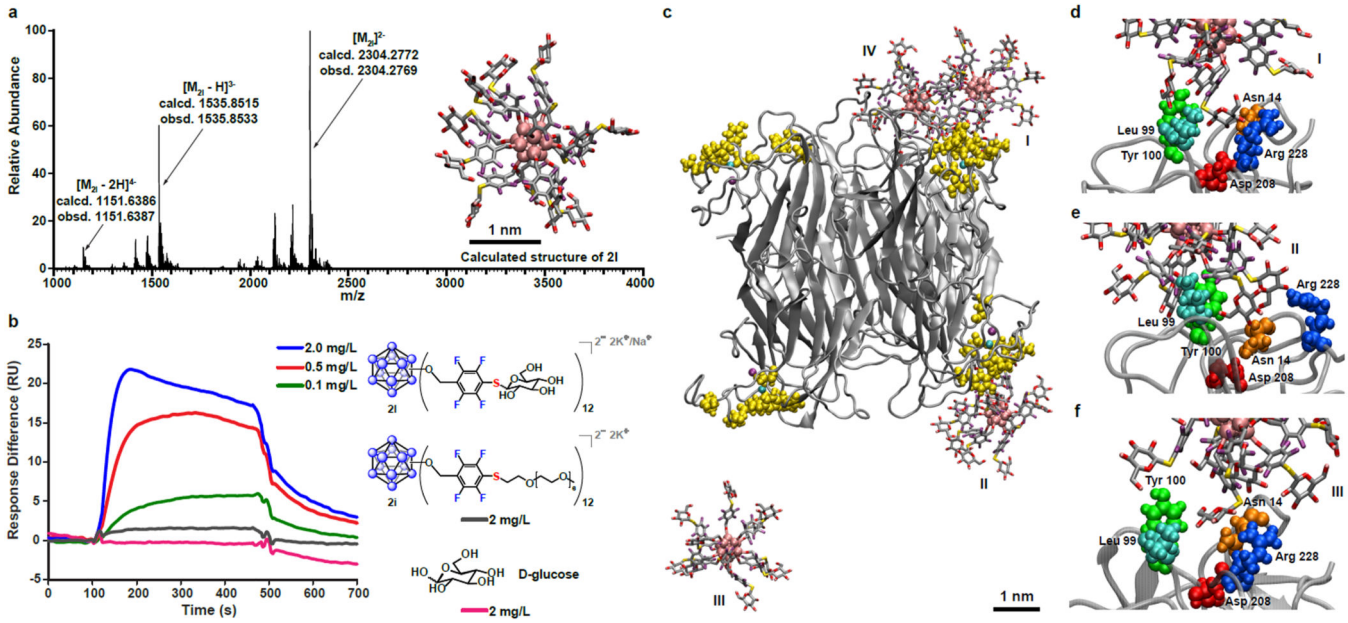


**Figure 4. Multivalent binding of the glycosylated OCN 2l to the lectin Concanavalin A (ConA)**

**a**, Electrospray ionization-high resolution mass spectrometry (ESI-HRMS) of **2l** supports its proposed structure and composition (see inset for the MD simulated structure of **2l** in aqueous environment). **b**, Surface plasmon resonance (SPR) sensorgram indicates that the measured binding response is dependent on the concentration of **2l**. Furthermore, it suggests multivalent binding interactions between **2l** and ConA as well as minimal binding of the PEGylated cluster **2i** and D-glucose controls to ConA. **c**, A snapshot at 20 ns of a MD simulation showcases the interactions between four **2l** particles (I, II, III, IV) and ConA. **d–f**, MD simulation close-up snapshots of three of the **2l** particles (I, II, III) binding to ConA at the known monosaccharide-binding residues (colored and labeled). See the Supplementary Information for the movie illustrating this simulation and another movie illustrating the weakly binding interactions between D-glucose and ConA.

## Table 1

Conjugation Scope for 2 and 3.

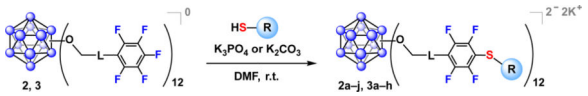


| Entry | Symbol | L | R | Time (h) | *in situ* yield[a] (%) | Isolated yield[b] (%) |
|---|---|---|---|---|---|---|
| 1 | **2a** | none |  | 24 | 99 | 70 |
| 2 | **2b** | none |  | 24 | 99 | 90 |
| 3 | **2c** | none | 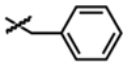 | 24 | 99 | 94 |
| 4 | **2d** | none | 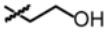 | 24 | 99 | 40 |
| 5 | **2e** | none | 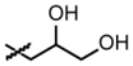 | 24 | 99 | 30 |
| 6 | **2f** | none | 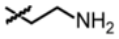 | 24 | 99 | 49 |
| 7 | **3a** |  |  | 7[c] | 99 | 87 |
| 8 | **3b** |  |  | 7[c] | 99 | 85 |
| 9 | **3c** | 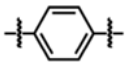 | 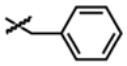 | 5 | 99 | 81 |
| 10 | **3d** |  |  | 2 | 99 | 81 |
| 11 | **3e** |  | 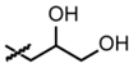 | 4 | 99 | 59 |
| 12 | **3f** | 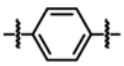 | 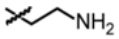 | 3 | 99 | 33 |
| 13 | **3g** | 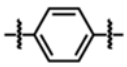 | 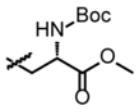 | 3 | 99 | 49 |
| 14 | **3h**[d] |  | 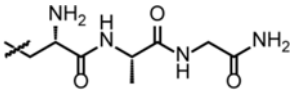 | 6 | 99 | 29 |

[a] Yield determined by $^{19}F$ NMR spectroscopy.

[b] Isolated yields after purification.

[c] Small scale reactions show full conversion within 1 hour.

[d] Additional 36 eq. isopropoxytrimethylsilane ($^{i}$PrMe$_3$Si) was employed to scavenge fluoride ($F^-$) by-product.

**Table 2**

PEGylation and glycosylation of 2 and 3.

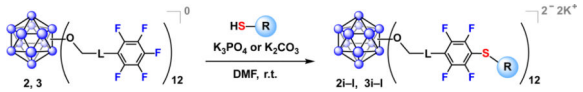


| Entry | Symbol | L | R | Time (h) | *in situ* yield[a] (%) | Isolated yield[b] (%) |
|---|---|---|---|---|---|---|
| 1 | **2i** | none | 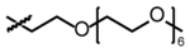 | 24 | 99 | 81 |
| 2 | **2j** | none | 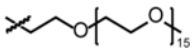 | 24 | 99 | 19 |
| 3 | **2k** | none | 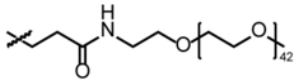 | 24 | 99 | 41 |
| 4 | **2l**[c] | none | 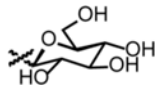 | 24 | 99 | 17 |
| 5 | **3i** |  | 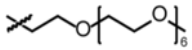 | 5 | 99 | 78 |
| 6 | **3j** |  | 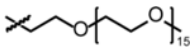 | 4 | 99 | 21 |
| 7 | **3k** | 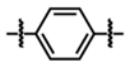 | 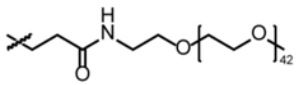 | 20[d] | 99 | 54 |
| 8 | **3l**[c] |  | 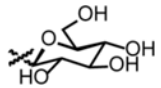 | 5 | 99 | 32 |

[a] Yield determined by $^{19}$F NMR spectroscopy.

[b] Isolated yields after purification.

[c] **2l** and **3l** have undergone partial $K^+/Na^+$ counterion exchange during the deprotection reaction with NaOMe.

[d] Small scale reaction shows full conversion within 5 hours.